Functionally graded composite cathodes for solid oxide fuel cells

N.T. Hart[a], N.P. Brandon[b,*], M.J. Day[a,1], N. Lapeña-Rey[a]

[a]*Rolls-Royce Strategic Research Centre, P.O. Box 31, Derby, DE24 8BJ, UK*
[b]*Department of Chemical Engineering and Chemical Technology, Imperial College of Science Technology and Medicine, London, SW7 2BY, UK*

Abstract

Functionally graded solid oxide fuel cell (SOFC) cathodes have been prepared from mixtures of strontium-doped lanthanum manganite (LSM) and gadolinia-doped ceria (CGO) using slurry spraying techniques. Similar samples were also prepared from mixtures of LSM and yttria-stabilised zirconia (YSZ). A current collector comprising a mixture of LSM and strontium-doped lanthanum cobaltite (LSCO) was then applied to both cathode types. Samples were characterised using scanning electron microscopy (SEM) and electrochemical impedance spectroscopy (EIS). Characterisation using EIS techniques showed that cathodes incorporating CGO into the structure gave improved performance over those fabricated using YSZ. These performance gains were most noticeable as the temperature was decreased towards 700 °C, and were maintained during the testing of three cell membrane electrode assemblies fabricated to the Rolls-Royce design.
© 2002 Elsevier Science B.V. All rights reserved.

Keywords: Solid oxide fuel cell; Functionally graded interfaces; Composite cathodes; Spraying

1. Introduction

Functionally graded materials (FGMs) have been developed as a method of joining dissimilar materials that are usually incompatible [1]. Instead of an abrupt change in composition and/or microstructure between the two materials, FGMs have a graded interface at which the composition gradually changes from one material to the other. The objective of this work is to apply this concept to the cathode of a solid oxide fuel cell (SOFC) using four materials, yttria-stabilised zirconia (YSZ), strontium-doped lanthanum manganite (LSM), gadolinia-doped ceria (CGO), and strontium-doped lanthanum cobaltite (LSCO).

The use of a mixed LSM–YSZ layer at the cathode–electrolyte interface to improve electrochemical performance is well-known. Such electrodes are referred to as composite cathodes and were first reported by Kenjo and Nishiya [2]. It was shown that by adding 50 wt.% YSZ to the LSM cathode, the polarisation resistance could be reduced to 25% of its original value. Subsequent studies showed improvements using a variety of cathode arrangements and fabrication methods [3–10].

Previous work has reported improvements by using grading techniques in SOFCs [11–15]. Hart et al. have recently demonstrated the effect of grading LSM–YSZ cathodes using screen printing fabrication techniques [15]. This showed that increasing levels of grading improved cathode performance. However, the highly graded structures produced are more complex, and therefore, more costly to fabricate. Incorporation of a more active material for oxygen reduction may offer similar performance gains, but without the need for such highly graded structures.

CGO is a candidate material for this application. Typically the ionic conductivity of CGO is of the order of magnitude of 50×10^{-3} S cm^{-1} at SOFC operating temperatures [16–18]. This is higher than the typical corresponding ionic conductivity of YSZ [19]. The difference is more pronounced at lower temperatures, e.g. at 700 °C the conductivity of CGO is 5.8×10^{-3} S cm^{-1} as compared to 1.4×10^{-4} S cm^{-1} for YSZ.

It has been reported that there is no known reaction between doped ceria and LSM [20] although a reaction between $Ce_{0.6}Gd_{0.4}O_{1.8}$ and YSZ has been reported to occur at temperatures above 1300 °C [21].

Previous workers have reported a polarisation resistance of 1.06 Ω cm^2 at 700 °C using a composite $Ce_{0.8}Gd_{0.2}O_2$–LSM cathode [20]. This was fabricated using a spin coating process on single crystal YSZ substrates and the final structure had a thickness of 20 mm. The aim of this

* Corresponding author. Tel.: +44-20-7594-5704;
fax: +44-20-7594-5604.
E-mail address: n.brandon@ic.ac.uk (N.P. Brandon).
[1] Present address: Advanced Ceramics Ltd., Castleworks, Stafford, ST16 2ET, UK.

investigation is to evaluate the improvement that could be obtained by using CGO in a cathode structure suited to manufacture at low cost using wet fabrication methods. The aim is to simplify the graded structure, so as to increase performance whilst maintaining a low manufacturing cost. CGO–LSM composite cathodes were therefore manufactured and their performance compared to an equivalent cathode fabricated using an LSM–YSZ composite layer.

2. Experimental procedure

Two cathode types were fabricated, one incorporating an LSM–YSZ composite, the other an LSM–CGO composite. In both cases, an LSCO current collector was used. Details of the materials used are given in Table 1. Cathodes were fabricated using three sprayed layers and a doctor bladed current collector. The cathode structure is schematically illustrated in Fig. 1. The first layer comprises a mixture of 50 wt.% LSM1 and 50 wt.% YSZ or CGO, the second layer an intermediate LSM2 current collector, the third a composite of 40 wt.% LSM2 and 60 wt.% LSCO1, with the top layer being the LSCO2 current collector. Table 2 summarises the composition of the samples prepared.

Each sprayed layer had a thickness of around 10 μm. The current collector thickness was approximately 150 μm. Cathodes were fired at temperatures of either 1125 or 1150 °C for 1 h. A ramp rate of 3 °C min^{-1} was used up to 500 °C to allow the binder to burn out, and 5 °C min^{-1} thereafter.

Cathodes were deposited either as half-cells onto both sides of dense 200 μm thick YSZ substrates (TZ8Y, Tosoh, Japan) for electrochemical impedance spectroscopy (EIS) measurements, or onto three cell multi-cell membrane electrode assemblies (MEA) for fuel cell performance testing. Details of the Rolls-Royce multi-cell MEA design are given in [22], and the cell is schematically illustrated in Fig. 2.

Table 1
Powders used to prepare composite cathodes

Powder	Composition	Particle size d$_{50}$ (μm)
YSZ	$(Zr_2O_3)_{0.92}(Y_2O_3)_{0.08}$	3.2
LSM1	$La_{0.85}Sr_{0.15}Mn_{1.1}O_3$	1.2
LSM2	$La_{0.85}Sr_{0.15}Mn_{1.1}O_3$	4.3
LSCO1	$La_{0.84}Sr_{0.16}CoO_3$	5.6
LSCO2	$La_{0.84}Sr_{0.16}CoO_3$	8.7
CGO	$Ce_{0.9}Gd_{0.1}O_3$	2.9

Table 2
Summary of cathode samples prepared[a]

Sample	YSZ-1125	YSZ-1150	CGO-1125	GCO-1150
Layer 1	LSM50:Y50SS	L50:Y50SS	L50:Y50SS	L50:Y50SS
Layer 2	L100SS	L100SS	L100SS	L100SS
Layer 3	L40:LC60SS	L40:LC60SS	L40:LC60SS	L40:LC60SS
Layer 4	LC100DB	LC100DB	LC100DB	LC100DB
Sintering details	1125 °C (1 h)	1150 °C (1 h)	1125 °C (1 h)	1150 °C (1 h)
Layer thickness	175 μm	170 μm	160 μm	175 μm

[a] Layers screen printed unless otherwise noted SS: slurry sprayed; DB: doctor bladed L: LSM, Y: YSZ, LC: LSCO, 50 = 50 wt.%, 100 = 100 wt.%.

Cross sections of all samples were coated with carbon and examined using a JOEL JXA 840A scanning electron microscope with an acceleration voltage of 20 kV. Fracture surfaces were examined to characterise the microstructure and identify any cracks or delamination.

Electrochemical impedance spectroscopy measurements were carried out over a range of temperatures using a Schlumberger 1260 frequency response analyser. The experimental procedure has been described in [15]. Measurements were taken without a dc bias, and spectra were obtained in the 10 mHz–500 kHz frequency range with an applied voltage amplitude of 20 mV. All the samples were measured in air at temperatures increasing from 700 to 1000 °C in 50 °C intervals. All data measured on the cathode half-cells were corrected for electrode area, and divided by two to obtain the actual polarisation resistance.

Three cell MEA testing was carried out using an alumina test holder, illustrated in Fig. 3. The holder was mounted in a muffle furnace (Lenton Thermal designs, UK), and provided with fuel, air, and electrical connections. The three cell MEA was sealed into the holder using a glass ceramic tape. Electrical connections to the end terminals of the MEA were made using ceramic sheathed platinum wire, held in place by a ceramic block. A thermocouple was placed above the MEA surface to measure sample temperature. Gas composition was controlled via thermal mass flow controllers (Hi-Tek). Fuel gases were hydrated to around 3% water by bubbling through water at 298 K using Dreschel bottles, before entering the test rig at a flow rate of 200 ml min^{-1}. Cell performance was measured using a scanning galvanostat (Sycopel Scientific, UK) to control the current though all three cells. The potential across all three cells was measured as a function of temperature and current density using a digital voltmeter.

— 100% LSCO
— 60% LSM / 40% LSCO
— 100% LSM
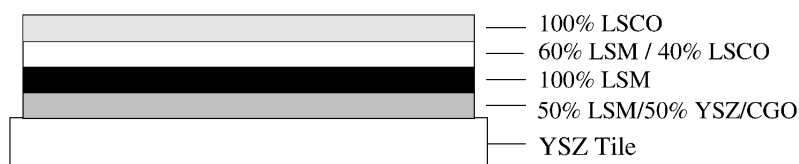— 50% LSM/50% YSZ/CGO
— YSZ Tile

Fig. 1. Schematic diagram of one side of the cathode half-cell structure used to evaluate the LSM–YSZ and LSM–CGO composite cathodes.
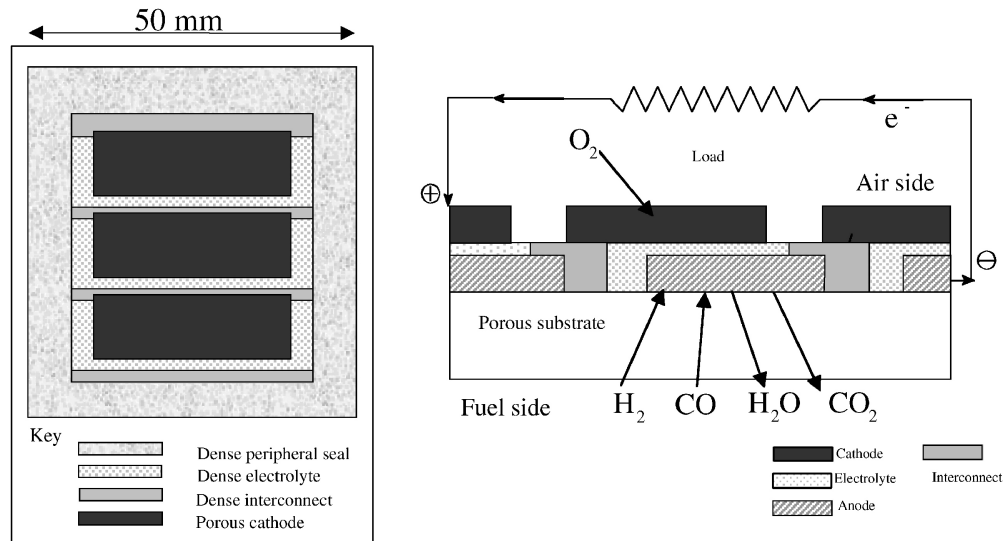
Fig. 2. Schematic illustration of the three cell membrane electrode assembly fabricated to the Rolls-Royce IP-SOFC design.
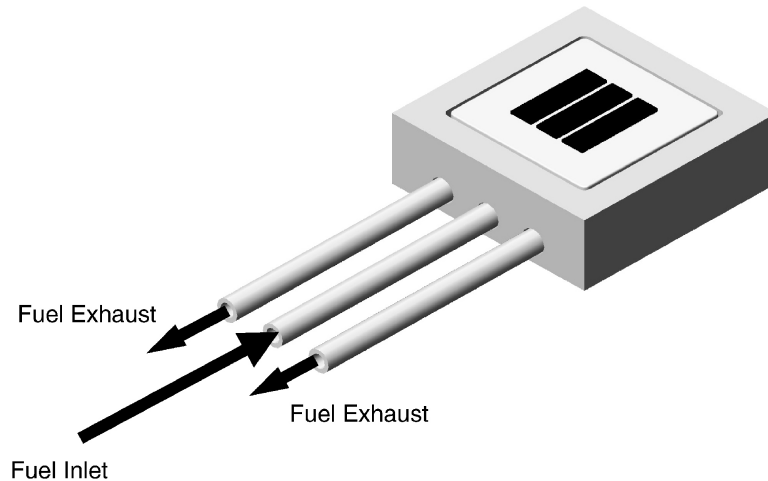

Fig. 3. Illustration of the three cell test holder.

3. Results

3.1. Cathode half-cell testing

Scanning electrode microscopy (SEM) microscopy revealed that the microstructure of all the samples was similar. An example of the cross section of a fracture surface of sample CGO-1125 (Fig. 4a) illustrates the fine microstructure of the sprayed layers next to the dense electrolyte, and the coarse microstructure of the doctor-bladed LSCO layer. The LSCO layer had a high level of agglomeration, 10–20 μm in size, with high level of interconnected porosity. A higher magnification image of the cathode–electrolyte interface of this sample is shown in Fig. 4b. This indicates that neck formation had occurred between adjacent particles, and there was evidence that smaller particles had coalesced to form larger aggregates. There was a high level of interconnected porosity and there appeared to be good

adhesion with the dense YSZ tile. The microstructure of the composite layers sintered at 1150 °C showed evidence of the higher temperature treatment (Fig. 5). The aggregates formed from the smaller particles were slightly larger, and there was greater bonding with the dense YSZ tile.

Fig. 6a and b illustrates typical EIS responses, in this case from samples YSZ-1125 and CGO-1125 at 700 °C, respectively. The response from both samples comprises more than one contributing element, an arc at low frequencies (1 Hz–1 kHz) and a smaller arc at higher frequencies. Peak frequencies correspond to approximately 50 Hz and 10 kHz, respectively. As the temperature increased, the total impedance of the arc decreased, and at 850 °C the contributing arcs were not clearly distinguishable, as illustrated by Fig. 7a and b. The frequency at which the peak of the arc occurred was approximately 1 kHz.

Fig. 8a and b shows the effect of sintering at temperatures of 1125 and 1150 °C on the EIS response from both samples.
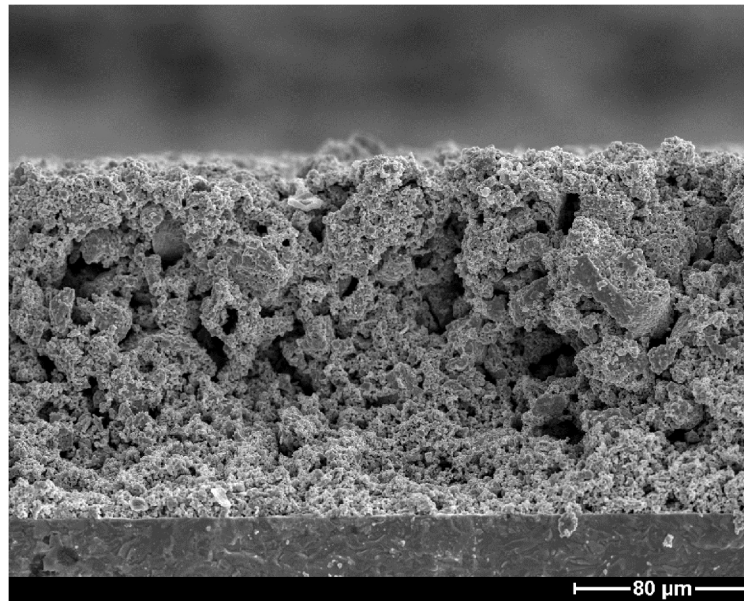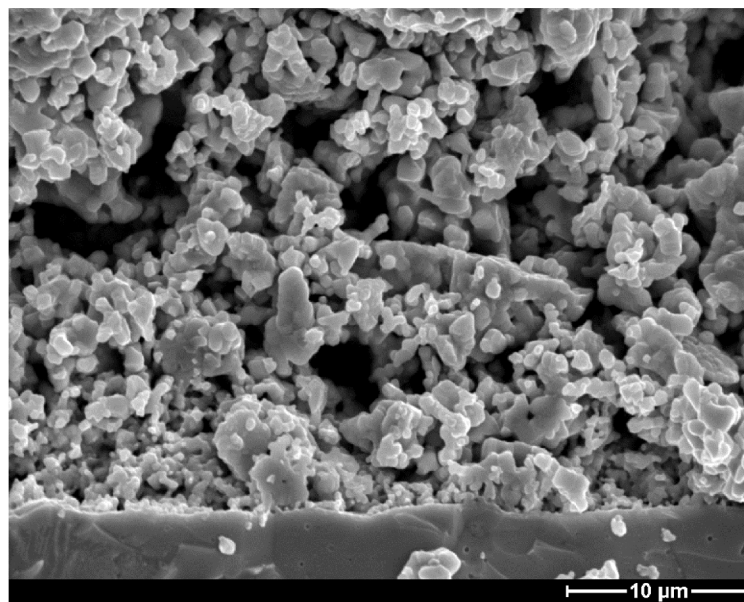
Fig. 4. SEM micrograph of a fracture surface of the LSM–CGO cathode sintered at 1125 °C showing (a) the whole cathode structure, and (b) the microstructure of the LSM–CGO region.

As the sinter temperature was increased, the low frequency arc increased in diameter, whilst the high frequency arc was largely unaffected. This trend was maintained throughout the temperature range studied.

The EIS arcs for the samples prepared with the YSZ composite layer were modelled using an equivalent circuit with three distributed elements, similar to that reported in [15]. Each element has an associated exponent value, phi, which reflects its displacement from the real axis. Values of phi of 0.95, 0.75 and 0.69 were used for the first, second and third element, respectively. These corresponded to the low,

mid and high frequency regions of the arc and are referred to accordingly. In a similar fashion to the previously reported study [15], the series resistance was evaluated in the fitting procedure, and the inductive component was set at 0.7×10^{-7} H.

The samples prepared with a CGO composite layer were treated using a variation of this approach. One equivalent circuit component was used to model the low frequency arc, visible at temperatures 850 °C and above. The main arc was fitted using two distributed elements. A value of 1 was fixed for phi corresponding to the very low frequency arc (referred
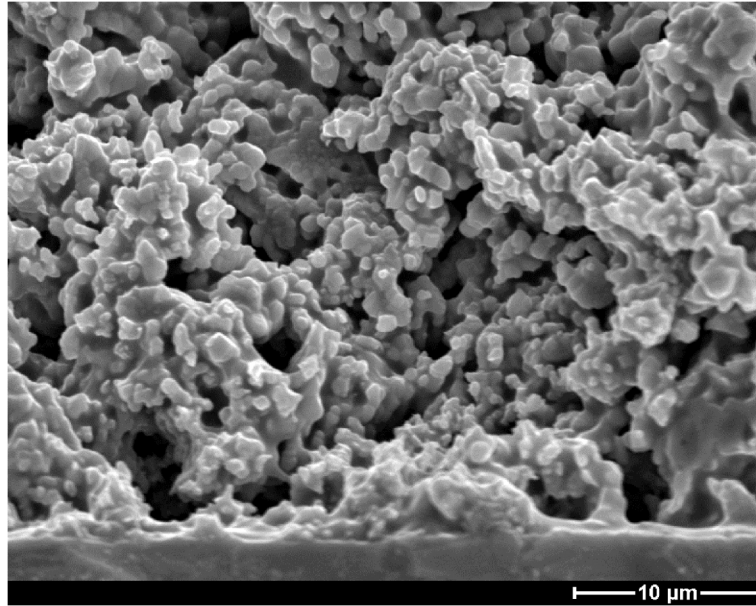
Fig. 5. SEM micrograph of a fracture surface of the LSM–CGO cathode sintered at 1150 °C.

to as low+), and values of 0.9 and 0.6 were used for the main arc (referred to as low and high, respectively). A non-linear least squares regression procedure was then used to fit the experimental data to the relevant equivalent circuit, and the fitted data then summarised in the form of Arrhenius plots.

There was little deviation between the measured series resistance for all the samples. This would tend to indicate that the sprayed composite layer did not significantly affect the performance of the electrolyte, and that the ionic conductivity of the YSZ was not reduced by an adverse reaction with the CGO.

Fig. 9 illustrates the effect of sinter temperature on the total polarisation resistance (being the sum of the low+, low,

mid and high frequency components as appropriate) of both samples types. The decrease in polarisation resistance from the use of the lower sintering temperature was evident across the temperature range in both cases. At 700 °C the samples prepared with YSZ gave a polarisation resistance of 12.1 and 16.4 Ω cm^2 for samples sintered at 1125 and 1150 °C, respectively. These values decreased to 1.88 and 2.27 Ω cm^2 at 850 °C, and 0.27 and 0.34 Ω cm^2 at 1000 °C. The cathodes with a CGO composite layer sintered at 1125 °C provided reduced polarisation resistances of 1.74, 0.202 and 0.037 Ω cm^2 at temperatures of 700, 850 and 1000 °C, respectively. When sintered at 1150 °C, these values increased to 2.15, 0.26 and 0.038 Ω cm^2.
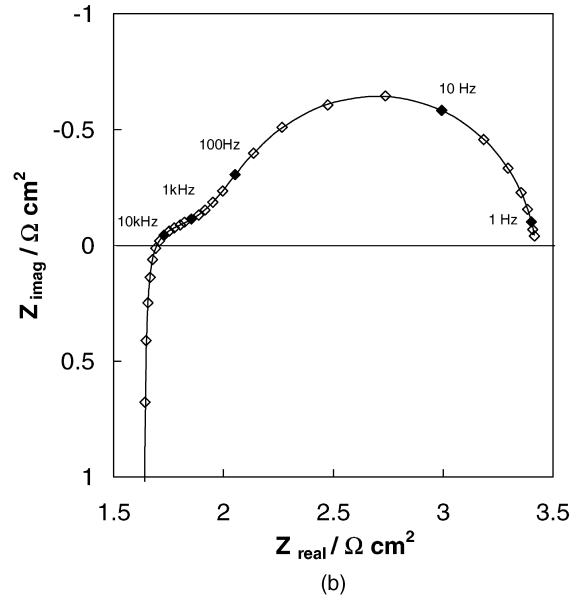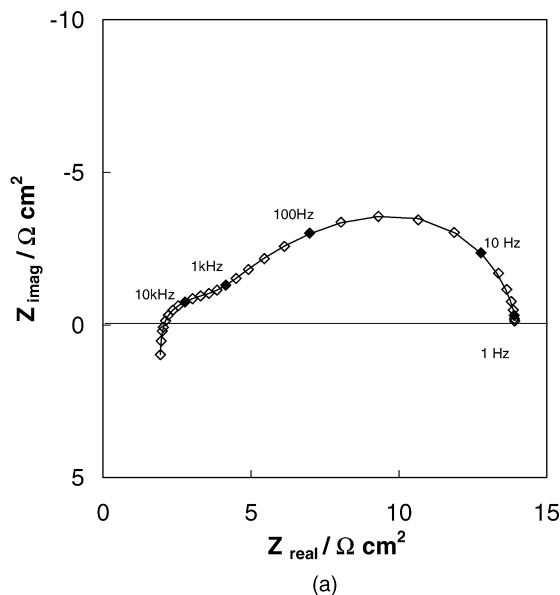

Fig. 6. EIS response of cathodes sintered at 1125 °C and measured in air at 700 °C, (a) LSM–YSZ and (b) LSM–CGO.
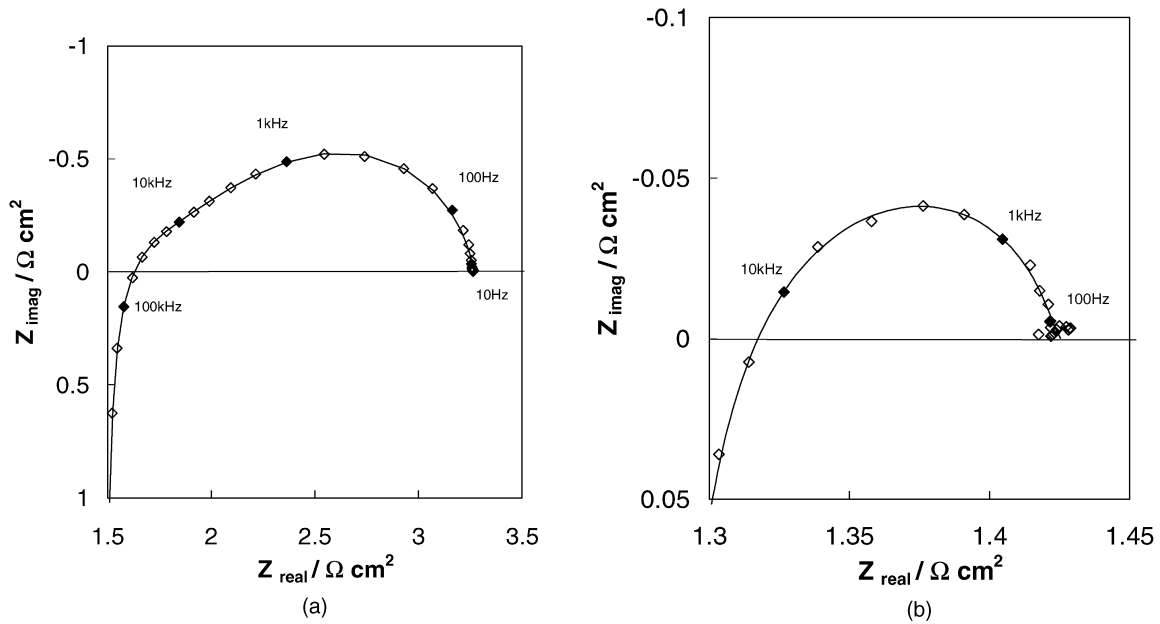
Fig. 7. EIS response of cathodes sintered at 1125 °C and measured in air at 850 °C, (a) LSM–YSZ and (b) LSM–CGO.

Fig. 9 also illustrates that the activation energy of the reaction at both the CGO–LSM and YSZ–LSM cathodes was similar, indicating that the overall reaction mechanism did not strongly depend on the nature of the ionic component within the composite cathode. There is evidence of an increase in activation energy at temperatures above 850 °C. This behaviour is similar to, but less marked than, that reported in previous work on screen printed YSZ–LSM graded cathodes [15].

The mid and high frequency contributions to the overall polarisation resistance showed little effect of sinter temperature. In fact the low frequency elements of the EIS arcs most clearly illustrate the benefits of using a lower sintering temperature, as shown in Fig. 10. This region of the EIS response therefore appears to reflect some physical change

in the cathodes due to the higher sinter temperature, such as a decrease in contact area between the ionic and electronic components. Both sets of samples show similar trends, though again the CGO based cathodes show enhanced performance. The activation energy was 1.5 eV across the temperature range. The magnitude of the very low frequency arc seen in the CGO–LSM samples at high temperatures was essentially independent of temperature over the range 850–1000 °C, suggesting it was related to gas phase diffusion within the cathode pores. While the area specific resistance associated with this feature was small, it was higher for samples sintered at 1150 °C than for those sintered at 1125 °C, i.e. 7 mΩ cm^2 compared to 5 mΩ cm^2, respectively. This is likely to reflect a reduction in porosity at the higher sintering temperature.
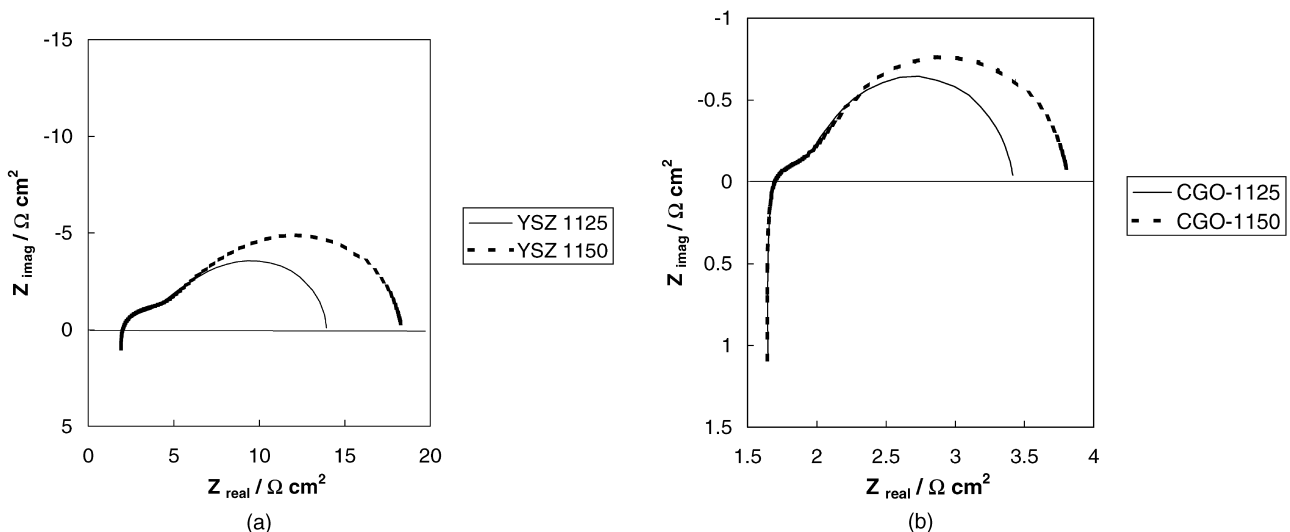

Fig. 8. Comparison of the EIS response of cathodes sintered at 1125 and 1150 °C, and measured in air at 700 °C, (a) LSM–YSZ and (b) LSM–CGO.
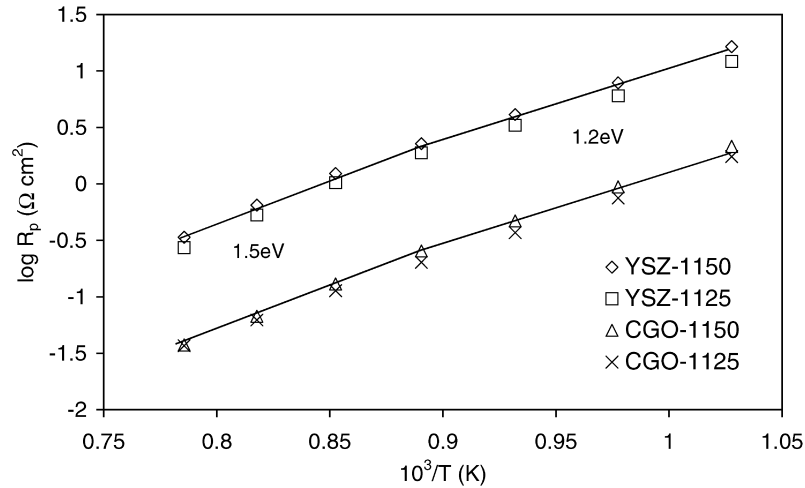
Fig. 9. Arrhenius plot of the polarisation resistance of LSM–YSZ and LSM–CGO cathodes sintered at 1125 and 1150 °C and measured in air.

3.2. Three cell membrane electrode assembly testing

To evaluate the effect of these results on a fully operational fuel cell, both the YSZ–LSM and CGO–LSM cathodes were applied to a three cell membrane electrode assembly. The cathode structures were fabricated in an identical fashion to the half-cells, and the performance measured under operational conditions. Samples were only prepared using the lower sintering temperature of 1125 °C and performance was measured at temperatures of 750–950 °C in 50 °C intervals. Results were taken from open circuit to an applied current density of 0.33 A cm^{-2}.

The results of the cell test are shown in Fig. 11. Three regions are distinguishable within the current–voltage curve, namely a sharp drop in voltage at low current levels due to activation polarisation, followed by a linear region where ohmic losses dominate, and then a fall in cell voltage at higher currents due to mass transport limitations.

Fig. 11 clearly demonstrates the benefits of the CGO–SM composite cathode layer over the YSZ–LSM composite cathode, particularly at lower operating temperatures. The improvement offered by the use of CGO is small at temperatures above 900 °C, but as the temperature decreases, the benefits increase. This behaviour reflects the temperature dependence of the ionic conductivity of CGO and YSZ, which both display similar values of ionic conductivity at high temperatures, with the conductivity benefit of the CGO becoming increasingly evident with decreasing temperature.

A least squares fit procedure was used to estimate the gradient of results in both the low and mid current regions. The results of the mid current region of the I–V curve, which is dominated by ohmic losses in the cell, showed that the resistance increased from approximately 1.0 Ω cm^2 at 950 °C to 1.6 Ω cm^2 at 750 °C (see Table 3). Both samples behaved similarly. This is not surprising, because in this region the resistance is dominated by the current collectors
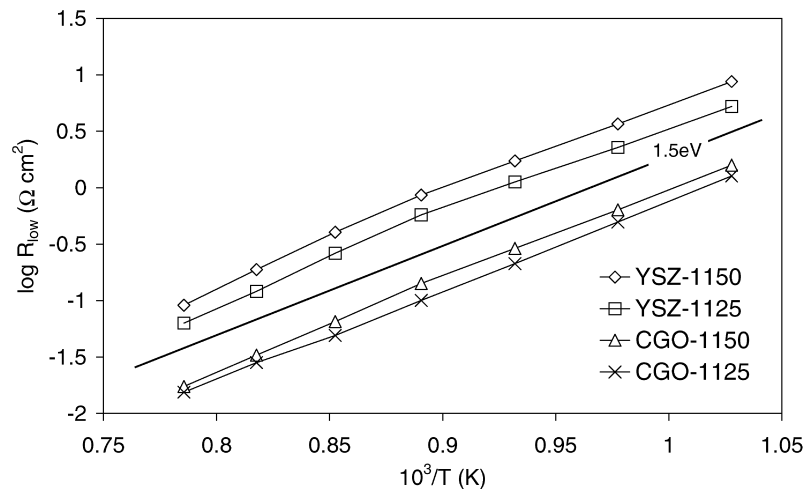

Fig. 10. Arrhenius plot of the low frequency contribution to the polarisation resistance of LSM–YSZ and LSM–CGO cathodes sintered at 1125 and 1150 °C and measured in air.
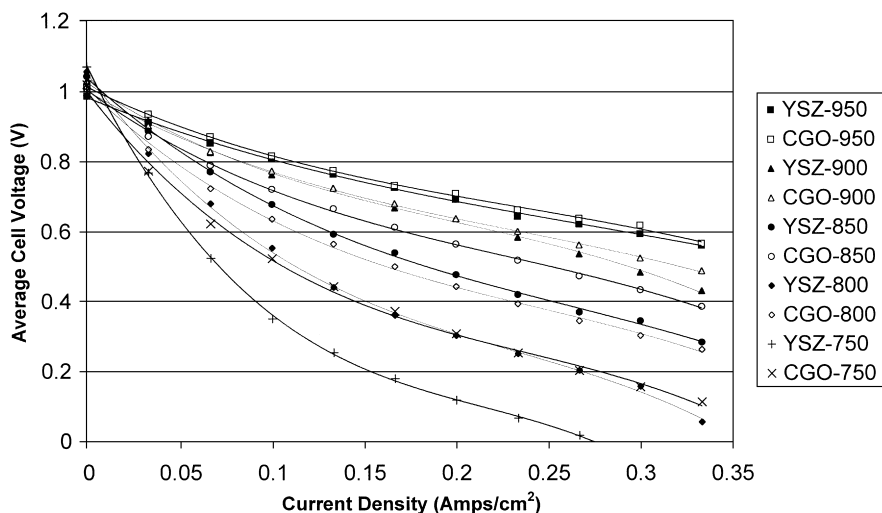
Fig. 11. Mean cell voltage against current density for three cell MEAs fabricated using LSM–YSZ (YSZ) or LSM–CGO (CGO) cathodes, and measured in 97% H_2/3% H_2O–air at temperatures of 950, 900, 850, 800 and 750 °C.

Table 3
Effect of temperature on the area specific resistance of the linear (ohmic) region of the current-voltage curve obtained when testing three cell membrane electrode assemblies using 97% H_2/3% H_2O–air

Temperature (°C)	MEA with YSZ composite layer (Ω cm^2)	MEA with CGO composite layer (Ω cm^2)
950	0.99	1.08
900	1.20	1.17
850	1.42	1.39
800	1.57	1.54
750	1.61	1.63

Table 4
Effect of temperature on the area specific resistance of the low overpotential (<50 mV) region of the current–voltage curve obtained when testing three cell membrane electrode assemblies using 97% H_2/3% H_2O–air

Temperature (°C)	MEA with YSZ composite layer (Ω cm^2)	MEA with CGO composite layer (Ω cm^2)
950	2.01	2.00
900	3.06	2.60
850	4.53	3.2
800	7.83	5.12
750	11.36	6.83

and the electrolyte, and both the anode and electrolyte are the same in both cell types. Furthermore, while the cathodes do differ near the cathode–electrolyte interface, both contain the same LSCO current collecting layer, and would therefore be expected to display similar lateral conductivity.

However, the results of the low current region of the *I–V* curve, which is dominated by the activation overpotential at both anode and cathode, highlights the benefits of using the CGO–LSM composite layer. This region reflects the catalytic nature of the electrodes. Table 4 summarises the resistance obtained from the slope of the current–voltage

curve at low overpotentials, i.e. <50 mV from the open circuit value. This demonstrates that, at the highest temperature of 950 °C, there was little difference in performance between the CGO–LSM and YSZ–LSM cathodes. However, as the temperature was lowered, the performance benefits arising from the incorporation of the CGO–LSM cathode became increasingly evident.

4. Conclusions

Use of a CGO–LSM composite layer at the electrolyte–cathode interface resulted in an improvement in performance when compared to a YSZ–LSM composite layer. Samples sintered at a temperature of 1125 °C had a lower level of grain growth in the composite layer. This resulted in an increase in active surface area, and decreased the polarisation resistance when compared to samples sintered at the higher temperature of 1150 °C.

The EIS spectra revealed several contributing components. At higher measurement temperatures, the samples prepared with the CGO–LSM composite layer revealed an arc at very low frequencies. This was not strongly temperature dependant, and is therefore likely to be related to the diffusion of oxygen through the porous cathode.

When the cathodes were tested in a three cell membrane electrode assembly, the EIS results correlated well with the cell activation resistances under operational conditions. At high temperatures, where the contribution made by the cathode polarisation resistance is relatively small, there was little benefit in moving towards a cathode with higher electrocatalytic activity. Under these conditions, diffusion processes appear to dominate cathode performance. However, as the operating temperature was reduced, the performance improvements offered by the use of the CGO–LSM cathode became significant.

Acknowledgements

References

[1] M. Koizumi, in: The concept of FGM, functionally gradient materials, Ceramic Trans., Am. Ceram. Soc. 34 (1993) 3.

[2] T. Kenjo, M. Nishiya, Solid State Ion. 57 (1992) 295.

[3] M.J.L. Ostergard, C. Clausen, C. Bagger, M. Mogensen, Electrochim. Acta 40 (1995) 1971.

[4] M. Juhl, S. Primdahl, C. Manon, M. Mogensen, J. Power Sources 61 (1996) 173.

[5] M.J. Jorgensen, S. Primdahl, M. Mogensen, Electrochem. Acta 44 (1999) 4195.

[6] P. Holtappels, M.J. Jorgensen, S. Primdahl, M. Mogensen, C. Bagger, in: Nantes, France P. Stevens (Eds.), Proceedings of the 3rd European SOFC Forum, June, 1998, p. 311.

[7] M. Juhl, S. Primdahl, M. Mogensen, in: Roskilde, Denmark F.W. Poulsen, N. Bonanos, S. Linderoth, M. Mogensen, B. Zachau-Christiansen (Eds.), Proceedings of the 17th Risoe International Symposium on Material Science, September, 1996, p. 295.

[8] E.P. Murray, T. Tsai, S.A. Barnett, Solid State Ion. 110 (1998) 235.

[9] T. Tsai, S.A. Barnett, Solid State Ion. 93 (1997) 207.

[10] M. Nagata, C. Iwasawa, Y. Seino, H. Yamamoto, M. Ono, in: Proceedings of the 2nd International Fuel Cell Conference, Kobe, Japan, Nedo, 1996, p. 255.

[11] K. Oizumi, L. Gauckler, Proc. Int. Symp. Stuct. Func. Grad. Mater 3 (1995) 651.

[12] K. Sasaki, M. Godickemeier, P. Bohac, A. Orliukas, L.J. Gaukler, in: Proceedings of the 5th IEA-Workshop SOFCs, Julich, Germany, 1993, p. 187.

[13] C. Bagger, S. Linderoth, M. Mogensen, P.V. Hendriksen, B. Kindl, S. Primdahl, P.H. Larsen, F.W. Poulsen, N. Bonanos, M.J. Jorgensen, in: S.C. Singhal, M. Dokiya (Eds.), Proceedings of the 6th International Symposium on SOFCs, Honolulu, Hawaii, October, Electrochem. Proc. 99–19 (1999) 28.

[14] M. Cassidy, C. Bagger, N. Brandon, M. Day, in: A.J. McEvoy (Ed.), Proceedings of the 4th European SOFC Forum, 10–14th July, Lucerne, Switzerland, 2000, p. 637.

[15] N.T. Hart, N.P. Brandon, M.J. Day, J.E. Shemilt, J. Mat. Sci. 36 (2001) 1077.

[16] B.C.H. Steele, Solid State Ion. 75 (1995) 157.

[17] B. Steele, Solid State Ion. 86–88 (1996) 1223.

[18] R. Doshi, V.L. Richards, J. Carter, X. Wang, M. Krumpelt, J. Electrochem. Soc. 146 (1999) 1273.

[19] U.G. Bossel, Facts and Figures, Swiss Federal Office of Energy, Berne, Switzerland, 1992.

[20] E. Murray, S. Barnett, in: S.C. Singhal, M. Dokiya (Eds.), Proceedings of the 6th International Symposium on SOFCs, Electrochemical Society, Pennington, NJ, 1999, p. 369.

[21] O.A. Mar'ina, S. Primdahl, C. Bagger, M. Mogensen, in: U. Stimming, S.C. Singhal, H. Tagawa, W. Lehnert (Eds.), Proceedings of the 5th International Symposium on SOFCs, Electrochemical Society, Pennington, NJ, 1997, p. 540.

[22] F.J. Gardner, M.J. Day, N.P. Brandon, M.N. Pashley, M. Cassidy, J. Power Sources 86 (2000) 122.